

Percolation of thermal conductivity in amorphous fluorocarbonsMarc G. Ghossoub,^{1,*} Jung-Hyun Lee,¹ Oksen T. Baris,¹ David G. Cahill,^{2,3} and Sanjiv Sinha^{1,4}¹*Department of Mechanical Science and Engineering, University of Illinois, Urbana, Illinois 61801, USA*²*Department of Materials Science and Engineering, University of Illinois, Urbana, Illinois 61801, USA*³*The Frederick Seitz Materials Research Laboratory, University of Illinois, Urbana, Illinois 61801, USA*⁴*Micro and Nanotechnology Laboratory, University of Illinois, Urbana, Illinois 61801, USA*

(Received 13 October 2010; published 23 November 2010)

We report experimental evidence of the percolation of thermal conductivity in nanometer scale thin films of amorphous fluorocarbon, using time-domain thermoreflectance measurements. According to the theory of Phillips and Thorpe, rigidity percolation in covalent glasses results in a power-law dependence of the elastic modulus on the average coordination number. Our measurements show that thermal conductivity behaves similarly. We derive the relation between thermal conductivity and coordination number from the rigidity percolation model using the theory of minimum thermal conductivity. Experiments verify the individual validity of each of these models in the film samples. This paper elucidates the physics of heat conduction in covalently bonded amorphous solids near the percolation threshold.

DOI: [10.1103/PhysRevB.82.195441](https://doi.org/10.1103/PhysRevB.82.195441)

PACS number(s): 65.60.+a, 62.20.de

I. INTRODUCTION

The Phillips-Thorpe^{1,2} model of rigidity percolation in covalently bonded solids separates amorphous solids from polymeric glasses based on the availability of zero-frequency vibrational modes in the glass. The number of zero-frequency modes is the difference between the total degrees of freedom and the rank of the dynamical matrix. Such modes enable the glass to be continuously deformed without any change in energy. Thorpe showed that above an average coordination number of 2.4, a glass no longer possesses zero-frequency modes and becomes an overconstrained system. Rigidity percolates in such a system and consequently the glass is converted to an amorphous solid. While measurements of the elastic constant show evidence of such percolation^{3–11} with measured thresholds^{12,13} ranging between 2.4 and 2.7, the impact on thermal conductivity is not clear.

The only connection to heat conduction reported thus far is for group-IV chalcogenide glasses.¹⁴ The measured thermal diffusivities for several chalcogenides exhibit a remarkable peak at the percolation threshold which corresponds to a 0.2 composition factor for the semiconductor. The threshold condition is believed to lower the resistance to thermal waves in this material. Apart from this, there is no direct measurement of thermal conductivity that shows lattice scale percolation. The usual percolation of thermal conductivity described in the literature^{15–18} is actually the percolation of thermal resistance which is typical of composites.

In this paper, we investigate the variation in thermal conductivity with decreasing thickness in amorphous fluorocarbon (a-C:F) films that are nanometer scale thin. A pump-probe thermoreflectance measurement¹⁹ provides the conductivity data. In analyzing x-ray photoelectron spectroscopy (XPS) data for the films, we find that the coordination number of carbon atoms changes as the film thickness decreases. Relating the change in thermal conductivity to the change in coordination number, we find a power-law relation between the two. We derive an identical power law using He

and Thorpe's²⁰ theory of rigidity percolation and the theory of minimum thermal conductivity.²¹ Picosecond acoustics data confirm the individual validity of each of these two models for the measured samples.

These results provide experimental verification of the model of rigidity percolation and quantitatively verify the threshold while introducing the concept of thermal-conductivity percolation that was suggested by Thorpe in his original paper but has not been experimentally verified. In particular, the extrapolated threshold from our data provides a near-perfect match with the value from Thorpe's theory. The thermal-conductivity data reported here are important in applications such as low-*k* dielectric materials in integrated circuits, biopassivation layers, low friction coatings, and adhesion promoters.

II. EXPERIMENT

In this section, we first describe the process for fabricating nanometer scale thin films of amorphous CF_x. The films range in thickness from 2 to 37 nm, as measured by ellipsometry and XPS. XPS data further provide the average coordination number. We describe a pump-probe reflectance measurement that provides thermal-conductivity data for the films. The picosecond scale reflectance data from the same measurement provide the speed of sound that is used to link rigidity and thermal-conductivity percolations in the next section.

A. Film fabrication and characterization

The average coordination number of carbon atoms in plasma deposited amorphous fluorocarbons changes with the deposited thickness provided the film thickness is less than ~30 nm. The choice of a moderate rf power for the plasma leads to a steady film deposition rate which is slow enough to deposit nanometer scale thick films.²² The films used in our measurements polymerized on a polished, clean silicon wafer from a CHF₃ monomer gas flowing at 80 SCCM (SCCM

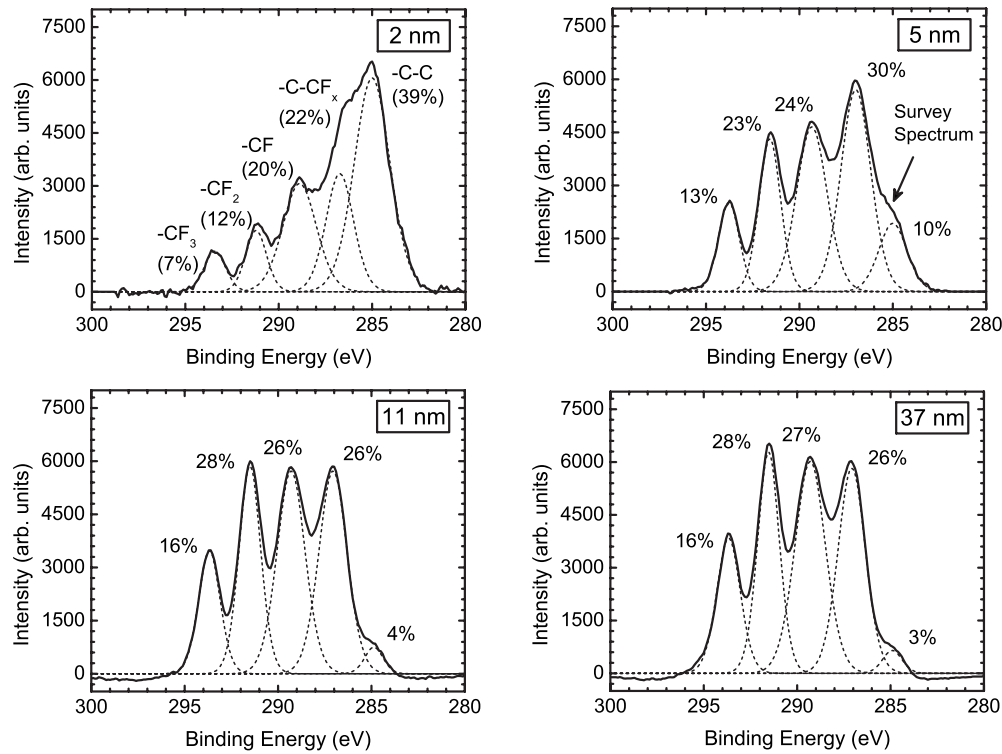


FIG. 1. C 1s core-level XPS spectra of the fluorocarbon films showing a change in film composition at different film thicknesses. Neglecting —C=C contribution, each —C—C functional group adds four sp^3 C—C covalent bonds to the overall sp^3 content of the fluorocarbon films. The —C—C functional group contribution to film chemical composition decreases from $\sim 39\%$ for the thinnest films (2 nm) to $\sim 3\%$ for the thickest (37 nm) which indicates a decrease in sp^3 content with increasing film thickness.

denotes cubic centimeter per minute at STP) with a base pressure of 150 mTorr and an rf plasma power of 80 W. The deposition rate was approximately 8.4 nm/min and remained independent of thickness for the films reported in this paper. The rf ionized CF_x gas radicals react with the Si surface and the surrounding gas phase to form a highly cross-linked network of —C—F_x ($x=1-3$) bonds, —C—C bonds, and —C—CF_x cross links.

Annealing the deposited films for 2 h at 250 °C reduced surface waviness. Atomic force microscopy measured the surface roughness after annealing to be ~ 0.5 nm, comparable to values reported previously.²³ Ellipsometry measured film thicknesses for films thicker than 8 nm but failed to generate unique fits for thinner films. The refractive indexes, n and k showed a thickness dependence that is expected for changes in film morphology and is consistent with data reported earlier.²³ XPS provided thickness measurements for films thinner than 8 nm. The thickness “ d ” of the fluorocarbon can be determined from its attenuation of the substrate signal at normal incidence and is given by²⁴

$$d = \lambda \ln \left(\frac{C_f}{C_s} + 1 \right), \quad (1)$$

where C_f and C_s are the atomic concentrations of the fluorocarbon and substrate, respectively, and λ is the inelastic

photoelectron mean-free path in the fluorocarbon. The mean-free path is approximately 3 nm.²⁵ XPS has been previously used to measure the thickness of SiO_2 ,²⁶ polymer,²⁷ and fluorocarbon²⁸ thin films. In determining film thickness by XPS, we assumed a uniform density for all thicknesses of the fluorocarbons. X-ray reflectivity measurements on the thin films revealed that the density does not show any significant dependence on thickness. The measured value is ~ 1.6 g/cm³ and is 27% smaller than the density of bulk PTFE (2.2 g/cm³) but is consistent with previous measurements for similar fluorocarbon films.²⁹

Analysis of the XPS data further provides the average coordination number of carbon atoms in the films as follows. XPS is able to detect distinct functional groups in the C—F system because of the wide separation (~ 2 eV) in their binding energies but is unable to distinguish between —C—C and —C—H bonded groups. It is known that CHF_3 breaks down predominantly into difluorocarbene (CF_2) and hydrofluoric acid.^{30,31} Further, CHF_3 deposited films do not exhibit a —C—H stretching intensity peak in their Fourier transform infrared spectra.^{22,32} Therefore, we neglect the hydrogen content in our films. Figure 1 shows the measured C 1s core-level XPS spectra of the fabricated films with distinct peaks characteristic of —C—C/—C=C , —C—CF_x , —CF— , —CF_2 , and —CF_3 functional groups.

The coordination number of carbon atoms is the ratio of the percentage of C—C covalent bonds from the C 1s

core-level XPS spectra of the film to the total number of possible bonds in the film. Each functional group has a central carbon atom to which a maximum of four other carbons can be connected. For instance, each $-\text{CF}_x-$ functional

group will contribute $4-x$ $-\text{C}-\text{C}'$ covalent bonds to the film structure out of four possible bonds. By taking the appropriate weighting factor for each functional group, we calculate the coordination number³³ from

$$\langle r \rangle = \frac{1 \times \% \text{CF}_3 + 2 \times \% \text{CF}_2 + 3 \times \% \text{CF} + 4 \times (\% \text{C} - \text{CF}_x) + 4 \times (\% \text{C} - \text{C})}{100}, \quad (2)$$

where $\% \text{CF}_x$ ($x=1, 2, 3$) corresponds to the percent contribution of group $-\text{CF}_x-$ to the overall chemical composition of the film as evaluated from the area under the Gaussian Lorentzian curve fits of the $-\text{CF}_x-$ intensity peaks. The XPS signal arises from approximately the top 7 nm of each film and the Si(2*p*) intensity peaks from the substrate completely vanish in thicker films. For films thicker than 7 nm, we obtain the average coordination number using a graded layer approximation.

Figure 2 shows the average coordination number $\langle r \rangle$ and density for various film thicknesses. The value is largest ($\langle r \rangle=3.35$) for the thinnest fluorocarbon (2 nm) and decreases with increasing thickness to ~ 2.7 for the thickest film. For the latter case, the measured value agrees well with previously reported values.²² The increase in $\langle r \rangle$ with decreasing thickness arises from the decreasing fluorine content in films thinner than ~ 15 nm. The fluorine to carbon ratio³³ is readily obtained from

$$\frac{F}{C} = \frac{(3 \times \% \text{CF}_3 + 2 \times \% \text{CF}_2 + 1 \times \% \text{CF})}{100}. \quad (3)$$

Figure 2 shows that this ratio decreases with thickness for films less than ~ 15 nm thick. The fluorine to carbon ratio is 0.65 for a 2 nm film and increases to 1.3 for the thickest (37 nm) film. The latter agrees with previously reported measurements²² on thicker CHF_3 fluorocarbon films. Finally, the XRD spectra of films thicker than 25 nm showed only a broad peak that is characteristic of an amorphous structure. This confirmed that these films are amorphous.

B. Thermal conductivity measurements

We used a time-domain thermoreflectance (TDTR) technique³⁴ to measure the thermal conductivity of the fluorocarbon films. Details of the setup and the technique are described elsewhere.³⁵ Briefly, a mode-locked Ti-sapphire laser generates femtosecond laser pulses at a peak wavelength of 785 nm and a repetition rate of 80.0 MHz that are focused on a 70–100 nm thick aluminum film sputtered on top of the fluorocarbon. The optical-absorption length “ ξ ” in aluminum is ~ 8 nm at this wavelength. The hot electrons generated at the surface diffuse further into the metal, gradually losing their energy to the lattice. The electron diffusion length in aluminum is close to ~ 40 nm.³⁶ The absorbed energy increases the temperature of aluminum and sets up an isotropic thermal stress which is then dissipated in the form of a strain pulse. The laser beam is split into pump and probe beams through a beamsplitter and both the relative optical path length and the relative power of the two beams are adjusted by using a mechanical delay stage and wave plates, respectively. The probe beam measures the time-dependent change in reflectance. We set the $1/e^2$ radius of the beam to 15 μm and the pump and the probe powers to ~ 14 mW and ~ 12 mW, respectively. Heat diffuses predominantly in a direction normal to the Al surface since the diameter of the pump (~ 30 μm) is two orders of magnitude larger than the combined thickness of the aluminum and fluorocarbon films (~ 200 nm). In the following discussion, we use the term “stack” to collectively refer to the layers of silicon, fluorocarbon, and aluminum.

A solution, in cylindrical coordinates, to the two-dimensional heat diffusion equation from a periodic Gaussian source provides an analytical fit to the thermoreflectance

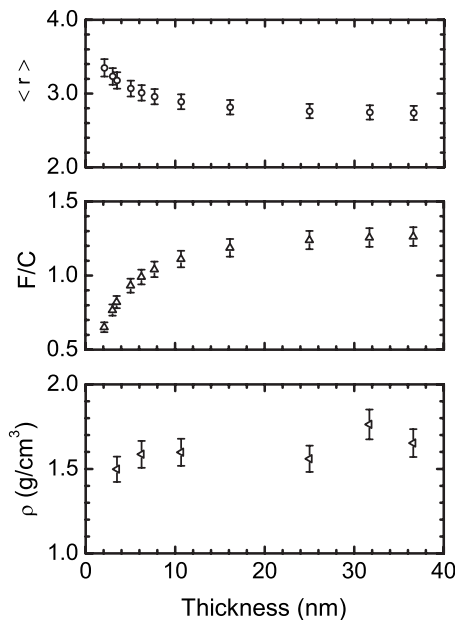


FIG. 2. The average fluorine to carbon ratio (F/C) increases with film thickness as more fluorine is incorporated in the thicker films. The average coordination number $\langle r \rangle$ follows an opposite trend as expected. The measured mass density is approximately independent of film thickness.

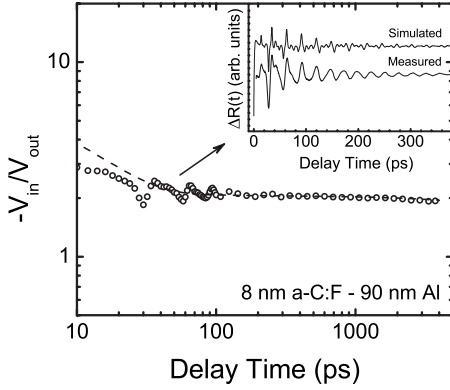


FIG. 3. Thermoreflectance curve and corresponding fit (dashed line) for 90 nm of aluminum on top of an 8 nm fluorocarbon film. The inset shows the picosecond acoustic peaks for the same sample. The speed of sound in the fluorocarbon and the thickness of aluminum are optimized to match the measured peaks and the corresponding decay with increasing delay time.

curve. We adopted a thermal model¹⁹ developed for determining the surface temperature of a multilayer and generated fits to the measured thermoreflectance curves by solving the model for known stack parameters and the unknown thermal conductivity of the film. Figure 3 shows a sample thermoreflectance curve for an 8 nm thick film and the corresponding fit from theory.

For each fluorocarbon thickness, an optimum aluminum film thickness was chosen to ensure a high sensitivity^{37,38} of the thermoreflectance curve to the thermal conductivity of the fluorocarbon film. The measurement's sensitivity to the thermal conductance of the fluorocarbon-silicon thermal interface was significant for the range of fluorocarbon thicknesses under investigation. The fitted thermal conductivity of the fluorocarbon layer decreased for increasing interface thermal conductance and no fit existed for interface conductances larger than 320 MW/m² K. We set the interface conductance to 320 MW/m² K such that we are effectively estimating the lower bound on the thermal conductivity. We do not expect significant change in the a-C:F/Si thermal interface across the different film thicknesses as all films were deposited under similar plasma conditions. The model did not show a significant sensitivity to the heat capacity of the fluorocarbon film which we fixed to be the value of bulk PTFE.

C. Measurement of the speed of sound

The reflectance signal from the pump-probe measurements includes an acoustic component that is distinct from the heat diffusion component in being oscillatory. The acoustic peaks, clearly visible in Fig. 3, are due to longitudinal strain pulses that are excited in aluminum and are reflected back from the interface with the rest of the stack. We used the acoustic peaks to determine the longitudinal speed of sound in the fluorocarbon films and the thickness of the aluminum transducer, as discussed below. More comprehensive discussions of the measurement technique and the underlying theory are available elsewhere.^{39–41}

Briefly, we extracted the acoustic peaks from the thermoreflectance curve by fitting the slowly decaying thermal background to a series of exponential functions and subtracting it from the data. We compared the extracted peaks to numerical calculations of the strain-dependent reflectivity change at the surface. The reflectivity change ΔR is

$$\Delta R(t) = \int f(z) \eta_{33}(z, t) dz, \quad (4)$$

where $f(z)$, the “sensitivity function,” determines how strain at different depths below the surface contributes to the change in the reflectivity. A detailed expression for $f(z)$ in metals is provided elsewhere.³⁹ The solution of the equations of elasticity for the layered medium provides the longitudinal component of the elastic strain tensor, η_{33} as³⁹

$$\eta_{33}(z, t) = (1 - R) \frac{Q\beta}{A\xi C} \frac{1 - \nu}{1 + \nu} r \left[e^{-z/\xi} + \frac{1}{2} e^{-|z+vt|/\xi} \text{sgn}(z + vt) + \frac{1}{2} e^{-|z-vt|/\xi} \text{sgn}(z - vt) \right], \quad (5)$$

where Q is the energy per pulse, R is the reflectivity, β is the linear-expansion coefficient, A is the illuminated area, and C is the specific heat per unit volume of aluminum. ν is Poisson's ratio and v is the longitudinal speed of sound in aluminum. The factor r represents the effective acoustic reflection coefficient⁴⁰ at the Al/a-C:F interface.

The inset of Fig. 3 shows the measured and the calculated acoustic peaks for a 90 nm aluminum transducer sputtered on top of an 8 nm a-C:F film. The calculations assume that no attenuation occurs in the fluorocarbon film. The model requires the thickness, the density, and the longitudinal speed of sound of individual layers as inputs. We fixed the speed of sound in aluminum to the bulk value of 6.42 nm/ps and varied the speed of sound in the fluorocarbon as well as the aluminum thickness to obtain the best fit.

The calculated acoustic peaks agree well with the measured peaks in both amplitude and delay time. The experimental peaks are distinctly broader than the fits which may be due to surface roughness in the fluorocarbon films that is not taken into account in the simulations. For a-C:F film thicknesses less than 10 nm, we found good fits to the measured data assuming a uniform speed of sound in the fluorocarbon. For films thicker than 10 nm, we fixed the value of the speed of sound at the a-C:F/Si interface to the value determined in the thinnest films and varied the value of speed of sound at the Al/a-C:F to obtain the best fits.

We assume that each fluorocarbon film can be approximated by a graded layer structure and we obtain the average speed of sound in the thick films by taking the integrated average of the measured speed of sound at the Al/a-C:F interface over the thickness of the graded layer. We note that picosecond acoustics measures the average transit time in the fluorocarbon films and not the average speed of sound directly. In our calculations we use the inverse of the average transit time to obtain the speed of sound which is not the same as the average speed of sound in the mathematical sense. However, for an exponential decrease in the speed of

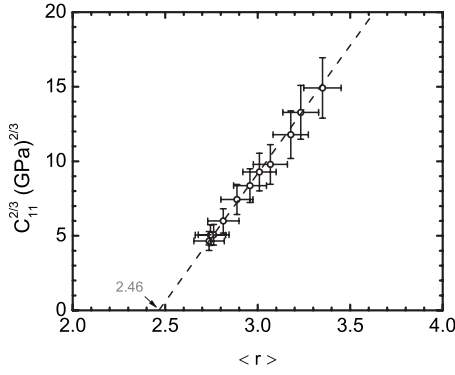


FIG. 4. Elastic modulus $C_{11}^{2/3}$ of a-C:F determined by picosecond acoustics vs coordination number $\langle r \rangle$ in these films as determined by XPS. The trend shows a power-law dependence that confirms the theory of rigidity percolation. The measured percolation threshold is 2.46 and agrees well with theory ($\langle r_c \rangle = 2.4$).

sound with fluorocarbon thickness, the two averages differ by less than 7% in the thickest films and hence, our approximation is well within the uncertainty of the measurement.

III. RESULTS AND DISCUSSION

He and Thorpe's²⁰ theory shows that the elastic modulus C_{11} has a power dependence on the coordination number beyond the rigidity percolation threshold ($\langle r_c \rangle = 2.4$),

$$C_{11} = 0.69 \left(\frac{\alpha}{4a} \right) (\langle r \rangle - 2.4)^{3/2}, \quad (6)$$

where α is a constant associated with the bond potential while $a/\sqrt{3}$ is the nearest-neighbor distance. In the continuum limit, the longitudinal speed of sound is $v_L = \sqrt{C_{11}/\rho}$. In our pump-probe measurements, the picosecond time scale reflectance data provides the speed of sound in the fluorocarbon films. We calculate the average coordination number from the XPS data as discussed in the section on measurements. Figure 4 plots the measured value of $C_{11}^{2/3}$ versus the coordination number $\langle r \rangle$ to clearly show the linear relationship, which is consistent with Eq. (6). In particular, the percolation threshold value of ~ 2.46 agrees remarkably well with the theoretical value of 2.4.

The above result establishes the presence of rigidity percolation in our films consistent with the Phillips-Thorpe model. We now explore the consequence of rigidity percolation on thermal conductivity. Thorpe had remarked in his original paper² that rigidity percolation should affect heat capacity and thermal conductivity but we are not aware of any subsequent work that establishes this link. In our measurements, the thermal conductivity k , increases with decreasing film thickness. Figure 5 shows the measured values as a function of measured film thickness. The thermal conductivity is $\sim 0.2 \text{ W m}^{-1} \text{ K}^{-1}$ for a 2 nm thick fluorocarbon and a factor of two larger than the thermal conductivity of the thickest (37 nm) deposited film. The measurements fall in the range of values reported for thin polymer films [e.g., $k \sim 0.2 \text{ W m}^{-1} \text{ K}^{-1}$ for poly(methyl methacrylate)] and ultrathin films of amorphous carbon⁴² (e.g., k

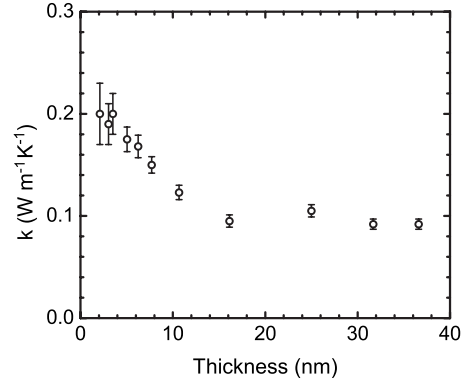


FIG. 5. The measured thermal conductivity of the fluorocarbons increases in the thinnest films to twice its value at 37 nm film thickness. Among other measurement uncertainties, the error bars account for the uncertainty in determining the density and heat capacity of the fluorocarbon films.

$\sim 0.1 \text{ W m}^{-1} \text{ K}^{-1}$ for a 0.9 nm thick tetrahedral amorphous carbon). The trend is remarkable given that the phonon mean-free path in the films is essentially the same as the bond length and is too short to cause any size dependence. Reconsidering the XPS data of Fig. 2, we find that the conductivity trend mirrors the change in coordination number with thickness. We show below that there is indeed a theoretical relation between thermal conductivity and the average coordination number assuming there is rigidity percolation.

The theory of minimum thermal conductivity²¹ in conjunction with rigidity percolation provides a straightforward relation for the percolation of thermal conductivity. The minimum thermal conductivity in an amorphous solid is given by

$$k_{\min} = \left(\frac{\pi}{6} \right)^{1/3} k_B n^{2/3} \sum_{i=1}^3 v_i \left(\frac{T}{\theta_i} \right)^2 \int_0^{\theta_i/T} \frac{x^3 e^x}{(e^x - 1)^2} dx, \quad (7)$$

where i is an index specifying all three sound modes, $\theta_i [= v_i (\hbar/k_B) (6\pi^2 n)^{1/3}]$ is the cutoff temperature associated with each mode, v_i the speed of sound and n the number density of atoms. In the high-temperature limit, k_{\min} scales as $n^{2/3} v_i$.

Combining Eqs. (6) and (7) and assuming a high-temperature limit, we find that the thermal conductivity above the threshold is related to the coordination number as

$$k = A (\langle r \rangle - 2.4)^{3/4} \quad (8)$$

where A is a material constant that includes density. The validity of the above relation rests on the individual validity of rigidity percolation and the minimum thermal conductivity in the amorphous solid.

We have already shown that rigidity percolates in the fluorocarbon films. We now test the validity of the theory of minimum thermal conductivity in these films. Since density is essentially constant across different films, the thermal conductivity should be linear in the speed of sound for the minimum thermal-conductivity theory to apply to each film. Figure 6 plots the measured thermal conductivity versus the measured speed of sound while the inset of Fig. 6 plots the

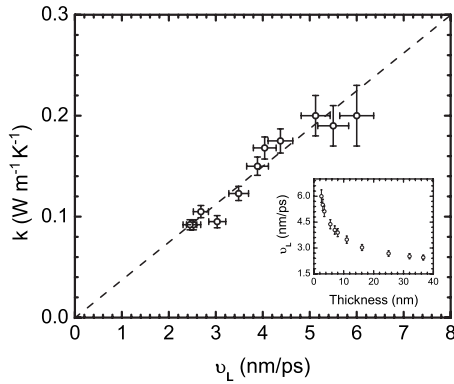


FIG. 6. The measured thermal conductivity scales linearly with the average longitudinal speed of sound in the films as determined by XPS. The inset shows the corresponding change in average longitudinal speed of sound as measured by picosecond acoustics. The speed of sound is three times larger in the thinnest films (~ 6 nm/ps) than its value at 37 nm. Among other measurement uncertainties, the error bars account for the uncertainty in determining the density and heat capacity of the fluorocarbon films.

measured average speed of sound as a function of film thickness. The measured linear relation between thermal conductivity and the speed of sound verifies the applicability of the theory of minimum thermal conductivity. We note that such agreement with the theory of minimum thermal conductivity has been experimentally verified for amorphous and hydrogenated carbon films^{42–46} in the past.

From Eq. (8), the thermal conductivity should obey a three-fourth power-law dependence on the average coordination number in amorphous solids. Figure 7 plots $k^{4/3}$ versus the coordination number $\langle r \rangle$. Since TDTR measures thermal resistances, the thermal conductivity plotted in Fig. 7 represents the inverse of the average thermal resistance and not the average thermal conductivity of the fluorocarbon films. However, as is the case for the speed of sound, the two averages differ by less than 7% in the thickest films and the approximation used is well within the measurement uncertainty. Furthermore, in deriving Eq. (8), we have assumed a homogeneous medium. This does not strictly apply to the graded layers of fluorocarbon. However, the error in averaging the right-hand side of Eq. (8) is less than 2% for our films. We find a reasonably good linear fit between $k^{4/3}$ and the average coordination number. The fit to the data intersects the coordination number axis at $\langle r \rangle = 2.43$, which is consistent with the expected percolation threshold of 2.4 from the Phillips-Thorpe theory.

We emphasize here that we have used three different combinations of measurements to independently verify the percolation of thermal conductivity, the applicability of minimum thermal conductivity and the percolation of rigidity. Specifically, time-domain thermoreflectance and XPS measurements provide evidence of thermal-conductivity percolation, time-domain thermoreflectance, and picosecond acoustics provide confirmation of minimum thermal conductivity, picosecond acoustics, and XPS provide evidence of rigidity percolation.

The percolation behavior of thermal conductivity in our samples is different from the percolation behavior of thermal

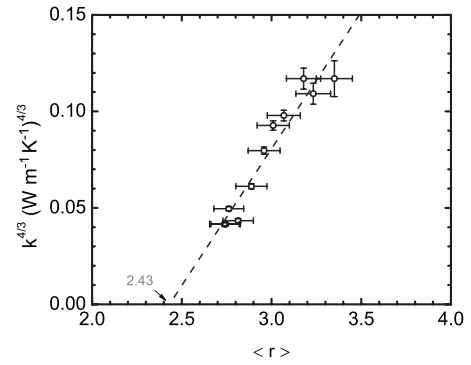


FIG. 7. The thermal conductivity of a-C:F shows a percolation threshold at an average coordination number of 2.43. The average coordination number is its value as determined by XPS and averaged over the thickness of the fluorocarbon.

diffusivity of chalcogenides¹⁴ where the diffusivity peaks at the threshold value. Here the thermal conductivity progressively decreases as the average coordination number approaches the threshold value. Recent measurements on nanostructured thermoelectric materials^{47,48} have drawn attention to the lower limit of thermal conductivity. As we see from our measurements, the theory of minimum thermal conductivity does not necessarily provide a lower numerical bound on thermal conductivity. In the case of amorphous solids, there is still room within the minimum thermal-conductivity regime to progressively decrease thermal conductivity at least until the percolation threshold. Measurements of k vs $\langle r \rangle$ at or below the threshold for glassy polymers remain unexplored. These measurements will likely provide insight into the thermal-conductivity behavior in that regime. Specifically for the measurements reported here, the thermal conductivity increases by $\sim 100\%$ even while obeying the minimum thermal-conductivity theory.

IV. CONCLUSION

In conclusion, we provide direct experimental evidence of thermal-conductivity percolation in thin films of amorphous fluorocarbon. The thermal conductivity varies as three-fourth power of the average coordination number. We obtain the same power-law dependence by combining the Phillips-Thorpe theory of rigidity percolation with the theory of minimum thermal conductivity. Our data suggest a percolation threshold at the coordination number of 2.4. Future experimental work on measuring thermal conductivity versus the coordination number in different organic materials close to or below the threshold value can provide a more complete picture of such percolation. Such lattice scale percolation physics can possibly be exploited in engineering materials to achieve tailored thermal conductivities.

ACKNOWLEDGMENTS

This work was carried out in part in the Frederick Seitz Materials Research Laboratory Central Facilities at the University of Illinois, which are partially supported by the U.S. Department of Energy under Grants No. DE-FG02-

07ER46453 and No. DE-FG02-07ER46471. M.G.G. and S.S. acknowledge support from the National Science Foundation through Grant No. NSF-CBET-09-54696-CAREER. D.G.C. acknowledges support from AFOSR MURI through

the grant MURI FA9550-08-1-0407. We particularly thank B. Daly for providing the software used in the picosecond acoustic simulations. We also thank R. Haasch for valuable discussions concerning the XPS measurements.

*ghossou1@illinois.edu

- ¹J. C. Phillips, *J. Non-Cryst. Solids* **34**, 153 (1979).
- ²M. F. Thorpe, *J. Non-Cryst. Solids* **57**, 355 (1983).
- ³W. Bresser, P. Boolchand, and P. Suranyi, *Phys. Rev. Lett.* **56**, 2493 (1986).
- ⁴B. L. Halfpap and S. M. Lindsay, *Phys. Rev. Lett.* **57**, 847 (1986).
- ⁵K. Tanaka, *Solid State Commun.* **60**, 295 (1986).
- ⁶S. S. Yun, H. Li, R. L. Cappelletti, R. N. Enzweiler, and P. Boolchand, *Phys. Rev. B* **39**, 8702 (1989).
- ⁷R. Bhadra, S. Susman, K. J. Volin, and M. Grimsditch, *Phys. Rev. B* **39**, 1378 (1989).
- ⁸X. Feng, W. J. Bresser, and P. Boolchand, *Phys. Rev. Lett.* **78**, 4422 (1997).
- ⁹A. C. Ferrari, J. Robertson, M. G. Beghi, C. E. Bottani, R. Ferulano, and R. Pastorelli, *Appl. Phys. Lett.* **75**, 1893 (1999).
- ¹⁰G. G. Naumis, *Phys. Rev. B* **73**, 172202 (2006).
- ¹¹R. P. Wang, A. Smith, B. Luther-Davies, H. Kokkonen, and I. Jackson, *J. Appl. Phys.* **105**, 056109 (2009).
- ¹²D. Selvanathan, W. J. Bresser, and P. Boolchand, *Phys. Rev. B* **61**, 15061 (2000).
- ¹³J. Y. Duquesne and G. Bellessa, *Europhys. Lett.* **9**, 453 (1989).
- ¹⁴J. Philip and K. N. Madhusoodanan, *Phys. Rev. B* **38**, 4127 (1988).
- ¹⁵A. Devpura, P. E. Phelan, and R. S. Prasher, *Microscale Thermophys. Eng.* **5**, 177 (2001).
- ¹⁶N. Shenogina, S. Shenogin, L. Xue, and P. Keblinski, *Appl. Phys. Lett.* **87**, 133106 (2005).
- ¹⁷P. Bonnet, D. Sireude, B. Garnier, and O. Chauvet, *Appl. Phys. Lett.* **91**, 201910 (2007).
- ¹⁸S. Kumar, M. A. Alam, and J. Y. Murthy, *Appl. Phys. Lett.* **90**, 104105 (2007).
- ¹⁹D. G. Cahill, *Rev. Sci. Instrum.* **75**, 5119 (2004).
- ²⁰H. He and M. F. Thorpe, *Phys. Rev. Lett.* **54**, 2107 (1985).
- ²¹D. G. Cahill and R. O. Pohl, *Solid State Commun.* **70**, 927 (1989).
- ²²E. J. Winder and K. K. Gleason, *J. Appl. Polym. Sci.* **78**, 842 (2000).
- ²³T. Easwarakhanthan, D. Beyssen, L. Le Brizoual, and J. Bougdira, *J. Vac. Sci. Technol. A* **24**, 1036 (2006).
- ²⁴K. R. Finnie, R. Haasch, and R. G. Nuzzo, *Langmuir* **16**, 6968 (2000).
- ²⁵C. D. Bain and G. M. Whitesides, *J. Phys. Chem.* **93**, 1670 (1989).
- ²⁶Z. H. Lu, J. P. McCaffrey, B. Brar, G. D. Wilk, R. M. Wallace, L. C. Feldman, and S. P. Tay, *Appl. Phys. Lett.* **71**, 2764 (1997).
- ²⁷K. C. Papat, S. Sharma, and T. A. Desai, *J. Phys. Chem. B* **108**, 5185 (2004).
- ²⁸N. R. Rueger, J. J. Beulens, M. Schaepkens, M. F. Doemling, J. M. Mirza, T. E. F. M. Standaert, and G. S. Oehrlein, *J. Vac. Sci. Technol. A* **15**, 1881 (1997).
- ²⁹L. Valentini, E. Braca, J. M. Kenny, L. Lozzi, and S. Santucci, *J. Vac. Sci. Technol. A* **19**, 2168 (2001).
- ³⁰K. P. Schug, H. Gg. Wagner, and F. Zabel, *Ber. Bunsenges. Phys. Chem.* **83**, 167 (1979).
- ³¹Y. Hidaka, T. Nakamura, and H. Kawano, *Chem. Phys. Lett.* **187**, 40 (1991).
- ³²S. J. Limb, K. K. Gleason, D. J. Edell, and E. F. Gleason, *J. Vac. Sci. Technol. A* **15**, 1814 (1997).
- ³³S. Tajima and K. Komvopoulos, *J. Phys. Chem. C* **111**, 4358 (2007).
- ³⁴H. K. Lyeo and D. G. Cahill, *Phys. Rev. B* **73**, 144301 (2006).
- ³⁵K. Kang, Y. K. Koh, C. Chiritescu, X. Zheng, and D. G. Cahill, *Rev. Sci. Instrum.* **79**, 114901 (2008).
- ³⁶G. Tas and H. J. Maris, *Phys. Rev. B* **49**, 15046 (1994).
- ³⁷R. M. Costescu, M. A. Wall, and D. G. Cahill, *Phys. Rev. B* **67**, 054302 (2003).
- ³⁸Y. K. Koh, S. L. Singer, W. Kim, J. M. O. Zide, H. Lu, D. G. Cahill, A. Majumdar, and A. C. Gossard, *J. Appl. Phys.* **105**, 054303 (2009).
- ³⁹C. Thomsen, H. T. Grahn, H. J. Maris, and J. Tauc, *Phys. Rev. B* **34**, 4129 (1986).
- ⁴⁰H. T. Grahn, H. J. Maris, and J. Tauc, *IEEE J. Quantum Electron.* **25**, 2562 (1989).
- ⁴¹C. J. Morath and H. J. Maris, *Phys. Rev. B* **54**, 203 (1996).
- ⁴²A. A. Balandin, M. Shamsa, W. L. Liu, C. Casiraghi, and A. C. Ferrari, *Appl. Phys. Lett.* **93**, 043115 (2008).
- ⁴³C. J. Morath, H. J. Maris, J. J. Cuomo, D. L. Pappas, A. Grill, V. V. Patel, J. P. Doyle, and K. L. Saenger, *J. Appl. Phys.* **76**, 2636 (1994).
- ⁴⁴M. Shamsa, W. L. Liu, A. A. Balandin, C. Casiraghi, W. I. Milne, and A. C. Ferrari, *Appl. Phys. Lett.* **89**, 161921 (2006).
- ⁴⁵J. L. Arlein, S. E. M. Palaich, B. C. Daly, P. Subramonium, and G. A. Antonelli, *J. Appl. Phys.* **104**, 033508 (2008).
- ⁴⁶A. J. Bullen, K. E. O'Hara, D. G. Cahill, O. Monteiro, and A. von Keudell, *J. Appl. Phys.* **88**, 6317 (2000).
- ⁴⁷A. I. Hochbaum, R. Chen, R. D. Delgado, W. Liang, E. C. Garnett, M. Najarian, A. Majumdar, and P. Yang, *Nature (London)* **451**, 163 (2008).
- ⁴⁸A. I. Boukai, Y. Bunimovich, J. Tahir-Kheli, J.-K. Yu, W. A. Goddard III, and J. R. Heath, *Nature (London)* **451**, 168 (2008).